Document downloaded from:

http://hdl.handle.net/10251/168881

This paper must be cited as:

García-Cortijo, S.; Gasulla Mestre, I. (2020). Universal Characteristic Equation for Multi-Layer Optical Fibers. IEEE Journal of Selected Topics in Quantum Electronics. 26(4):1-11. https://doi.org/10.1109/JSTQE.2020.2996375

The final publication is available at

https://doi.org/10.1109/JSTQE.2020.2996375

Copyright Institute of Electrical and Electronics Engineers

Additional Information

Universal characteristic equation for multi-layer optical fibers

S. García and I. Gasulla, *Senior Member, IEEE*

***Abstract*—Optical fibers featuring multi-layer refractive index profiles have been widely investigated and developed in a variety of scenarios, including space-division multiplexing transmission, fiber sensing, loss and dispersion management, as well as high-power amplifiers and lasers. For the first time to our knowledge, we present in this paper a general model deriving the universal characteristic equation for multi-layer optical fibers that comprise a set of concentric layers with arbitrary radial dimensions and refractive index values, considering both stepped (as step-index) or continuous (as graded-index) profiles. Expressions for the main fiber propagation parameters are also derived. We validate the model by comparing our results to the ones provided by numerical software tools with excellent matching for a series of particular optical fibers comprising step-index trench-assisted, ring-core, triangular-index and four-cladding profiles. This compact universal characteristic equation serves as a useful tool for optical fiber designers, where one can get valuable physical insights without the need to resort to numerical software tools, and even evaluate the effect of a single layer in isolation without the need to evaluate the whole refractive index structure.**

***Index Terms*— Optical fibers, optical fiber theory, optical propagation.**

I. Introduction

In its simplest form, an optical fiber comprises a single cylindrical core of doped silica glass surrounded by a pure-silica cladding whose refractive index is lower than that of the core, [1]. In the past 50 years, more complex index profiles have been developed beyond the simple step-index profile by incorporating different layers that act either as rings (higher refractive index than silica, up-doped with GeO_2 or P_2O_5 among others) or trenches (lower refractive index than silica, down-doped with fluorine or B_2O_3 among others) for different purposes, [2]. Representative examples of multilayer refractive index profiles are gathered in Fig. 1. For instance, the introduction of a down-doped intermediate layer between core and cladding gives rise to depressed-cladding fibers [3] (also named as W-type fibers [4-6]) and trench-assisted fibers, (see Fig. 1 (a) and (b)), allowing a stronger confinement of the mode than a usual single cladding fiber and thus reducing losses and intercore crosstalk in the case of multicore fibers. On the other hand, double-cladding fibers where the intermediate layer has a refractive index higher than the external cladding, have been developed mainly for high-power amplifiers and lasers [3,7], (see Fig. 1 (c)). Ring-core fibers find application in mode-division multiplexing system since they are able to minimize distributed intermodal coupling and thus reduce multiple input multiple output (MIMO) digital signal processing (DSP) complexity at reception [8-11], (see Fig. 1 (d)). In addition to step-index profiles, the core of the fiber can present a non-constant refractive index value, as the case of graded-index or triangular-index profiles. Fig. 1 (e) shows a graded-index trench-assisted fiber commonly used to decrease intermodal dispersion in mode-division multiplexing systems [12], while Fig. 1 (f) depicts a dispersion-shifted fiber with a triangular index profile incorporating a raised intermediate cladding or ring, [13]. More complex structures with a higher number of layers, such as four-cladding (or quadruple-cladding) fibers, can be found in different dispersion-flattened fibers, [14,15].

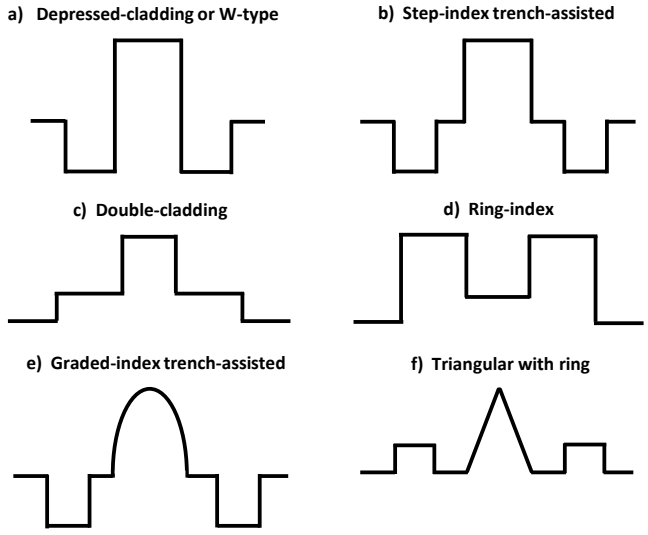

Fig. 1. Refractive index profiles of different optical fibers beyond step-index.

Fiber propagation of the electric and magnetic fields of optical waves is governed by the Maxwell equations and must satisfy the boundary conditions imposed at every interface between two refractive index layers. In the case of two-layer fibers (as single step-index or graded-index), the application of

Manuscript received October 12, 2019. This work is supported by the European Research Council (ERC) under Consolidator Grant Project 724663, the Spanish MINECO under TEC2016-80150-R project, BES-2015-073359 scholarship for S. García and Ramon y Cajal fellowship RYC-2014-16247 for I. Gasulla.

The authors are with the Photonics Research Labs of the iTEAM Research Institute, Universitat Politècnica de València, Camino de Vera s/n, Edificio 8G, 46022 Valencia. Spain. (e-mail: ivgames@iteam.upv.es).

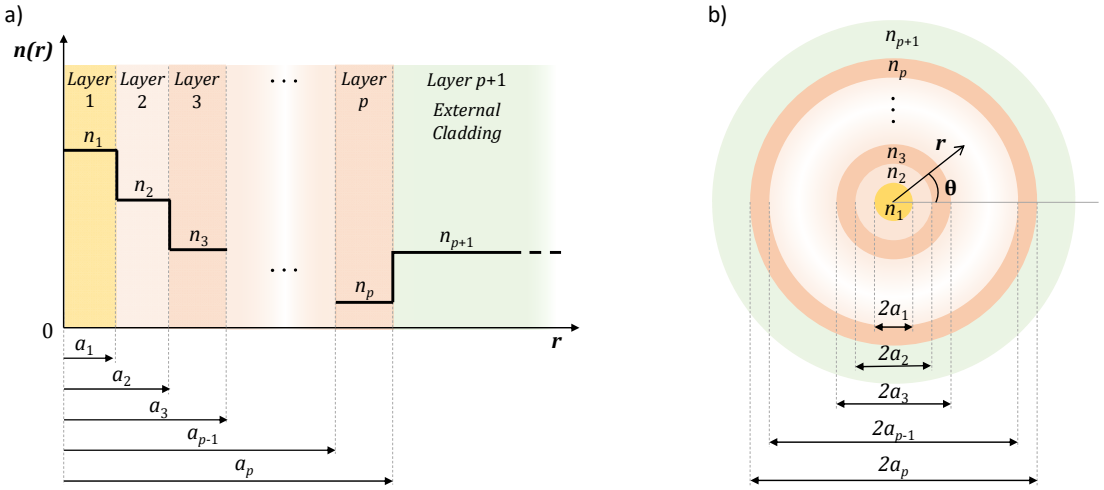

Fig. 2. a) Refractive index profile and b) cross-section area of a general multi-layer optical fiber with p+1 refractive index layers.

boundary conditions over weakly guided modes at the core-cladding interface $r = a$, (where a is the core radius), leads to the well-known compact form of the characteristic or eigenvalue equation, [16]. The solution of the characteristic equation requires graphical or numerical methods and provides the propagation constants of the different modes that propagate though the fiber. Beyond two layers, the characteristic equations of only a few three-layer refractive index profiles have been developed up to date: ring-core profile, [9]; step-index trench-assisted profile [17] where the characteristic equation is expressed in the form of a determinant; as well as double-cladding profile where the intermediate cladding has either a refractive index either lower (see Fig. 1 (a)) or higher (see Fig. 1(c)) than that of the external cladding, [3].

If the refractive index profile comprises a higher number of different radial layers, the derivation of the characteristic equation for the whole structure becomes a complex mathematical procedure that is usually not overtaken. Instead, one has to resort to numerical software tools to solve the modes that propagate through the fiber without having any valuable insight about the fiber propagation characteristics before running the software tool. We present in this paper the development of a general closed expression for the characteristic equation of multi-layer optical fibers with any number of layers, where each concentric layer has arbitrary radial dimensions and refractive index. This formula will play an important role in the design process of multi-layer optical fibers, providing a useful tool to obtain the phase propagation constant for all the propagated modes and to derive other propagation parameters such as the group delay or the chromatic dispersion.

Fig. 2 shows the refractive index profile as a function of the radial coordinate r and the cross-section area of a general optical fiber with p+1 concentric layers, where the layer p+1 behaves as the external cladding. Each layer k (k = 1, 2, …, p+1,) is characterized by a radius a_k, ($a_k > a_{k-1}$ for $k > 2$) and a refractive index value n_k that remains constant among each layer, that is, n_k (r) = n_k for $a_k > r > a_{k-1}$. Refractive index profiles that do not follow this flat-step structure, for instance those comprising graded or triangular shape sections, will be approximated by a multi-step structure where we discretize that continuous section into the required number of flat layers where n_k (r) = n_k. We will refer those cases as "continuous" refractive index profiles.

Section II provides the model that derives the general expression for the characteristic equation of the described multi-layer optical fibers. In section III, we determine the general expressions for the main propagation parameters that describe the modes propagating through multi-layer fibers. The validation of the model and its applicability are addressed in section IV by particularizing the generic expressions to specific refractive index profiles, considering both discrete and continuous refractive index profiles. Section V gathers further discussion about the application domain of the developed model. Finally, section VI closes the paper with the relevant conclusions and future directions of research.

II. Characteristic Equation for Multi-Layer Index Profiles

The general geometry and refractive index distribution of the multi-layer optical fiber we consider here are depicted in Fig. 2. We must take into account that the highest refractive index layer does not necessarily correspond to the first layer; it could be actually located in any layer between the first and the p^{th} layers. The outer cladding is assumed to extend to infinity in the radial dimension. Let n_{co} be the highest refractive index, n_{co} = $\max_{1\le i\le p}\{n_i\}$, and n_{clad} the refractive index of layer p+1, n_{clad} = n_{p+1}. In the following, we will consider weakly guiding fibers, assuming $n_{co} - n_{clad} << n_{co}$, [16]. Guided modes must then satisfy:

$$k_0 n_{clad} < \beta < k_0 n_{co}\,, \tag{1}$$

where k_0 is the vacuum wavenumber and β is the mode propagation constant. We must take into account that we assume dielectric optical fibers where the propagation constant β gets real values.

We use a cylindrical coordinate system (r,θ,z) and assume time- and z-dependent fields of the form exp(j(ωt - βz)). The axial field components are then expressed as [18]:

$$\begin{cases} E_z = f(r)\cos\left[(l+1)\theta\right], \\ H_z = n_1\sqrt{\dfrac{\varepsilon_0}{\mu_0}}f(r)\sin\left[(l+1)\theta\right], \end{cases} \tag{2}$$

being n_1 the refractive index in the central layer, and ε_0 and μ_0 the dielectric constant and the magnetic permeability in vacuum, respectively. In (2), the term $\exp(j(\omega t - \beta z))$ has been omitted for simplicity. Assuming weakly guidance approximation, guided modes can be approximated as linearly polarized modes, LP_{lm}, where the integer l corresponds to the azimuthal mode number and the integer m is the radial mode number that labels the roots for a given value of l. It is well known that each LP mode is composed of a set of degenerated modes: hybrid (HE and EH), TE, and TM modes, [16,18]. And, furthermore, each LP mode always degenerates at least into an HE mode, [16,18]. Due to this mode degeneracy, we particularized (2) for HE modes without loss of generality. The following analysis will then be focused on $HE_{l+1,m}$ modes, which after all define the $LP_{l,m}$ modes we are interested on, $l \geq 0$. The other degenerate modes can be trivially determined in a similar way.

Considering a refractive index profile structured around p dielectric discontinuities or layer interfaces, as shown in Fig. 2, for each refractive index layer k, $k = 1, 2, \ldots, p+1$, the radial function $f(r)$ for a particular azimuthal mode number l is given by, [19]:

$$f(r) = \begin{cases} A_1 B_{l+1}\left(\dfrac{x_1 r}{a_1}\right), & r < a_1, \quad k = 1, \\ A_{2(k-1)} B_{l+1}\left(\dfrac{x_k r}{a_1}\right) + A_{2(k-1)+1} V_{l+1}\left(\dfrac{x_k r}{a_1}\right), & a_{k-1} < r < a_k, \quad 1 < k \leq p, \\ A_{2p} V_{l+1}\left(\dfrac{x_{p+1} r}{a_1}\right), & r > a_p \quad k = p+1, \end{cases} \tag{3}$$

where A_i, $i = 1, 2, \ldots, 2p$, are arbitrary constants, the functions B_{l+1} represent the Bessel functions (or modified Bessel functions) of the first kind, $B_{l+1} = J_{l+1}$ (or $B_{l+1} = I_{l+1}$), the functions V_{l+1} represent the Bessel functions (or modified Bessel functions) of the second kind, $V_{l+1} = Y_{l+1}$ (or $V_{l+1} = K_{l+1}$), and the variables x_k are the normalized transverse propagation constants, $x_k = u_k$ (or $x_k = w_k$), of layer k. In the previous definitions, terms inside the parentheses are used when the corresponding layer acts as cladding, while terms without parentheses lead for core layers. That means that if the refractive index of layer k, n_k, is higher than the effective index of a given mode, n_{eff}, then this layer will act as core for that mode, while in the other case it will act as cladding. In other words, the core layers satisfy $\beta < k_0 n_k$, while the cladding layers satisfy $k_0 n_k < \beta$ (note the analogy to (1)). Table 1 summarizes, for each layer k and a given azimuthal mode number l, the corresponding: normalized transverse propagation constants x_k, auxiliary Bessel functions B_{l+1} and V_{l+1} that appear in the axial field components (see previous (3)), and auxiliary Bessel functions B_l and V_l that appear in the tangential field components (as we indicate later in (7)). For a better understanding, the identification of the Bessel functions (or modified Bessel functions) is shown in Fig. 3 (a), where, as an example, we show the particularization for layers 1 and 3 following Table 1 when considering two arbitrary propagating modes, named as modes a and b. The normalized transverse propagation constants for each layer k are expressed as

$$\begin{cases} u_k = k_0 a_1 \sqrt{n_k^2 - n_{eff}^2}, & n_{eff} < n_k, \\ w_k = k_0 a_1 \sqrt{n_{eff}^2 - n_k^2}, & n_{eff} > n_k. \end{cases} \tag{4}$$

TABLE I
BESSEL FUNCTIONS AND NORMALIZED TRANSVERSE PROPAGATION CONSTANTS OF LAYER K FOR A GIVEN AZIMUTHAL MODE NUMBER L

	$B_{l+1}(x_k)$	$V_{l+1}(x_k)$	$B_l(x_k)$	$V_l(x_k)$	x_k
$n_k > n_{eff}$	$J_{l+1}(x_k)$	$Y_{l+1}(x_k)$	$J_l(x_k)$	$Y_l(x_k)$	u_k
$n_k < n_{eff}$	$I_{l+1}(x_k)$	$K_{l+1}(x_k)$	$-I_l(x_k)$	$K_l(x_k)$	w_k

Once any of the transverse propagation constants in (4) is determined, the longitudinal mode phase propagation constant β is given by

$$\begin{cases} \beta^2 = (k_0 n_{eff})^2 = (k_0 n_k)^2 - (u_k / a_1)^2, & n_{eff} < n_k, \\ \beta^2 = (k_0 n_{eff})^2 = (w_k / a_1)^2 + (k_0 n_k)^2, & n_{eff} > n_k. \end{cases} \tag{5}$$

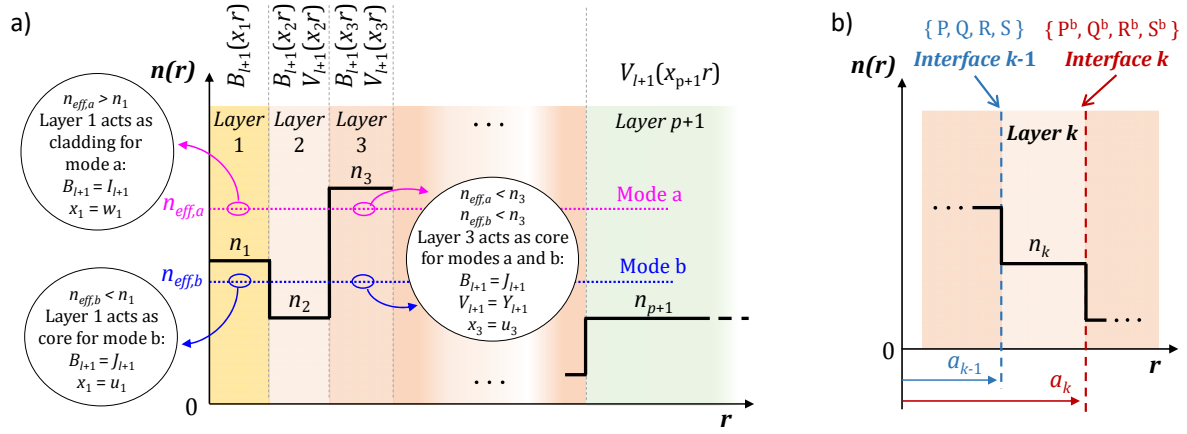

Fig. 3. a) Identification of Bessel functions in each refractive index layer and particularization for two modes (mode a and mode b) in layers 1 and 3; b) Identification of the minor determinants around the k-th refractive index layer.

Using Maxwell equations, we can derive the other field components from E_z and H_z as, [18],

$$\begin{aligned}\begin{pmatrix}E_\theta\\-E_r\end{pmatrix}&=\frac{1}{n_1}\sqrt{\frac{\mu_0}{\varepsilon_0}}\begin{pmatrix}-H_r\\-H_\theta\end{pmatrix}\\&=\frac{jn_1k_0}{\omega^2\varepsilon\mu-\beta^2}\left[f'(r)+(l+1)\frac{f(r)}{r}\right]\begin{Bmatrix}\sin[(l+1)\theta]\\\cos[(l+1)\theta]\end{Bmatrix},\end{aligned}\tag{6}$$

where ω is the angular optical frequency and $f'(r)$ is the derivative of $f(r)$ with respect to r. In order to maintain the generality of the expressions, we remain treating the radial function $f(r)$ on the general form introduced in (3) for the tangential field components. For simplicity, the derivatives of the generic Bessel functions B and V are treated as if they are Bessel functions of the first and second kinds, respectively, so a sign correction will be applied afterwards in the cladding regions due to Bessel functions derivative properties (see Table 1). The tangential field components result:

$$\begin{pmatrix}E_\theta\\-E_r\end{pmatrix}=jn_1k_0a_1\begin{Bmatrix}\sin[(l+1)\theta]\\\cos[(l+1)\theta]\end{Bmatrix}\cdot\begin{cases}A_1\dfrac{B_l\left(\frac{x_1r}{a_1}\right)}{x_1}, & r<a_1, \quad k=1,\\ A_{2(k-1)}\dfrac{B_l\left(\frac{x_kr}{a_1}\right)}{x_k}+A_{2(k-1)+1}\dfrac{V_l\left(\frac{x_kr}{a_1}\right)}{x_k}, & a_{k-1}<r<a_k,\ 1<k\le p,\\ A_{2p}\dfrac{V_l\left(\frac{x_{p+1}r}{a_1}\right)}{x_{p+1}}, & r>a_p \quad k=p+1.\end{cases}\tag{7}$$

The characteristic equation is derived by matching both the axial and the tangential field components at the dielectric discontinuities $r = a_j$, $j = 1, 2, \ldots, p$. From (2), (3) and (7), the continuity conditions of E_z, H_z, E_θ and H_θ lead to:

$$\mathrm{M}\begin{pmatrix}A_1\\A_2\\\vdots\\A_{2p}\end{pmatrix}=0,\tag{8}$$

where M is a $2p$ x $2p$ matrix in which odd rows come from the axial fields continuity and even rows come from the tangential fields' continuity. Existence of nontrivial solution to (8) leads to equate the determinant of the matrix M to zero, |M| = 0, that is,

$$\begin{vmatrix}
B_{l+1}(x_1) & B_{l+1}(x_2) & V_{l+1}(x_2) & 0 & 0 & \cdots & 0 & 0 & 0\\
\frac{B_l(x_1)}{x_1} & \frac{B_l(x_2)}{x_2} & \frac{V_l(x_2)}{x_2} & 0 & 0 & \cdots & 0 & 0 & 0\\
0 & B_{l+1}(\eta_2x_2) & V_{l+1}(\eta_2x_2) & B_{l+1}(\eta_2x_3) & V_{l+1}(\eta_2x_3) & \cdots & 0 & 0 & 0\\
0 & \frac{B_l(\eta_2x_2)}{x_2} & \frac{V_l(\eta_2x_2)}{x_2} & \frac{B_l(\eta_2x_3)}{x_3} & \frac{V_l(\eta_2x_3)}{x_3} & \cdots & 0 & 0 & 0\\
0 & 0 & 0 & B_{l+1}(\eta_3x_3) & V_{l+1}(\eta_3x_3) & \cdots & 0 & 0 & 0\\
0 & 0 & 0 & \frac{B_l(\eta_3x_3)}{x_3} & \frac{V_l(\eta_3x_3)}{x_3} & \cdots & 0 & 0 & 0\\
\vdots & \vdots & \vdots & \vdots & \vdots & \ddots & \vdots & \vdots & \vdots\\
0 & 0 & 0 & 0 & 0 & \cdots & B_{l+1}(\eta_{p-1}x_p) & V_{l+1}(\eta_{p-1}x_p) & 0\\
0 & 0 & 0 & 0 & 0 & \cdots & \frac{B_l(\eta_{p-1}x_p)}{x_p} & \frac{V_l(\eta_{p-1}x_p)}{x_p} & 0\\
0 & 0 & 0 & 0 & 0 & \cdots & B_{l+1}(\eta_px_p) & V_{l+1}(\eta_px_p) & V_{l+1}(\eta_px_{p+1})\\
0 & 0 & 0 & 0 & 0 & \cdots & \frac{B_l(\eta_px_p)}{x_p} & \frac{V_l(\eta_px_p)}{x_p} & \frac{V_l(\eta_px_{p+1})}{x_{p+1}}
\end{vmatrix}=0,\tag{9}$$

being $\eta_j = a_j/a_1$. After suppressing denominators in (9), the resulting determinant |M'| can be easily solved by cofactors. We start by solving |M'| by the cofactors of the last column ($2p$-th column), obtaining the two minor determinants as

$$\begin{aligned}|\mathrm{M}|=&x_pV_l(\eta_px_{p+1})\begin{vmatrix}B_{l+1}(x_1) & B_{l+1}(x_2)\cdots & 0\\ x_2B_l(x_1) & x_1B_l(x_2)\cdots & 0\\ \vdots & \vdots & \vdots\\ 0 & 0 & \cdots V_{l+1}(\eta_px_p)\end{vmatrix}\\&-x_{p+1}V_{l+1}(\eta_px_{p+1})\begin{vmatrix}B_{l+1}(x_1) & B_{l+1}(x_2)\cdots & 0\\ x_2B_l(x_1) & x_1B_l(x_2)\cdots & 0\\ \vdots & \vdots & \vdots\\ 0 & 0 & \cdots V_l(\eta_px_p)\end{vmatrix}.\end{aligned}\tag{10}$$

We now continue by solving the two determinants of (10) by cofactors of the first column, obtaining again two new minor determinants per each of the previous ones,

$$\begin{aligned}|\mathrm{M}|=&x_pV_l(\eta_px_{p+1})\left(x_1B_{l+1}(x_1)\begin{vmatrix}B_l(x_2)\cdots & 0\\ \vdots & \vdots\\ 0 & \cdots V_{l+1}(\eta_px_p)\end{vmatrix}-x_2B_l(x_1)\begin{vmatrix}B_n(x_2)\cdots & 0\\ \vdots & \vdots\\ 0 & \cdots V_n(\eta_px_p)\end{vmatrix}\right)-\\&x_{p+1}V_{l+1}(\eta_px_{p+1})\left(x_1B_{l+1}(x_1)\begin{vmatrix}B_l(x_2)\cdots & 0\\ \vdots & \vdots\\ 0 & \cdots V_l(\eta_px_p)\end{vmatrix}-x_2B_l(x_1)\begin{vmatrix}B_{l+1}(x_2)\cdots & 0\\ \vdots & \vdots\\ 0 & \cdots V_l(\eta_px_p)\end{vmatrix}\right)\\&=x_pV_l(\eta_px_{p+1})\left[x_1B_{l+1}(x_1)\mathbf{P}_2-x_2B_l(x_1)\mathbf{Q}_2\right]\\&-x_{p+1}V_{l+1}(\eta_px_{p+1})\left[x_1B_{l+1}(x_1)\mathbf{R}_2-x_2B_l(x_1)\mathbf{S}_2\right],\end{aligned}\tag{11}$$

where the variables $\mathbf{P}_2$, $\mathbf{Q}_2$, $\mathbf{R}_2$ and $\mathbf{S}_2$ refer to the resulting four minor determinants. While the range of the resulting determinants is higher than 2, the same procedure should be applied to expand again the preceding minor determinants by cofactors, starting again from the upper left corner but alternating row and column cofactors at each step. The recursive form of (11) satisfies then the following expressions for the minor determinants associated to the k-th layer, where $k = 2, 3, \ldots, p$-1,

$$\begin{cases} \mathbf{P}_k = B_l(\eta_{k-1}x_k)\mathbf{P}_k^b - V_l(\eta_{k-1}x_k)\mathbf{Q}_k^b \\ \mathbf{Q}_k = B_{l+1}(\eta_{k-1}x_k)\mathbf{P}_k^b - V_{l+1}(\eta_{k-1}x_k)\mathbf{Q}_k^b \\ \mathbf{R}_k = B_l(\eta_{k-1}x_k)\mathbf{R}_k^b - V_l(\eta_{k-1}x_k)\mathbf{S}_k^b \\ \mathbf{S}_k = B_{l+1}(\eta_{k-1}x_k)\mathbf{R}_k^b - V_{l+1}(\eta_{k-1}x_k)\mathbf{S}_k^b \end{cases}, \text{ layer } k, \text{ interface } k\text{-1}, \tag{12}$$

$$\begin{cases} \mathbf{P}_k^b = x_k V_{l+1}(\eta_k x_k)\mathbf{P}_{k+1} - x_{k+1} V_l(\eta_k x_k)\mathbf{Q}_{k+1} \\ \mathbf{Q}_k^b = x_k B_{l+1}(\eta_k x_k)\mathbf{P}_{k+1} - x_{k+1} B_l(\eta_k x_k)\mathbf{Q}_{k+1} \\ \mathbf{R}_k^b = x_k V_{l+1}(\eta_k x_k)\mathbf{R}_{k+1} - x_{k+1} V_l(\eta_k x_k)\mathbf{S}_{k+1} \\ \mathbf{S}_k^b = x_k B_{l+1}(\eta_k x_k)\mathbf{R}_{k+1} - x_{k+1} B_l(\eta_k x_k)\mathbf{S}_{k+1} \end{cases}, \text{ layer } k, \text{ interface } k.$$

The identification of these minor determinants around the k-th refractive index layer is shown in Fig. 3 (b). Finally, in the last iteration (i.e., for layer p), the last minor determinants $\mathbf{P}_p$, $\mathbf{Q}_p$, $\mathbf{R}_p$ and $\mathbf{S}_p$ are

$$\begin{cases} \mathbf{P}_p = \begin{vmatrix} B_l(\eta_{p-1}x_p)V_l(\eta_{p-1}x_p) \\ B_{l+1}(\eta_p x_p)V_{l+1}(\eta_p x_p) \end{vmatrix} \\ \quad = B_l(\eta_{p-1}x_p)V_{l+1}(\eta_p x_p) - V_l(\eta_{p-1}x_p)B_{l+1}(\eta_p x_p) \\ \mathbf{Q}_p = \begin{vmatrix} B_{l+1}(\eta_{p-1}x_p)V_{l+1}(\eta_{p-1}x_p) \\ B_{l+1}(\eta_p x_p) \quad V_{l+1}(\eta_p x_p) \end{vmatrix} \\ \quad = B_{l+1}(\eta_{p-1}x_p)V_{l+1}(\eta_p x_p) - V_{l+1}(\eta_{p-1}x_p)B_{l+1}(\eta_p x_p) \\ \mathbf{R}_p = \begin{vmatrix} B_l(\eta_{p-1}x_p)V_l(\eta_{p-1}x_p) \\ B_l(\eta_p x_p) \quad V_l(\eta_p x_p) \end{vmatrix} \\ \quad = B_l(\eta_{p-1}x_p)V_l(\eta_p x_p) - V_l(\eta_{p-1}x_p)B_l(\eta_p x_p) \\ \mathbf{S}_p = \begin{vmatrix} B_{l+1}(\eta_{p-1}x_p)V_{l+1}(\eta_{p-1}x_p) \\ B_l(\eta_p x_p) \quad V_l(\eta_p x_p) \end{vmatrix} \\ \quad = B_{l+1}(\eta_{p-1}x_p)V_l(\eta_p x_p) - V_{l+1}(\eta_{p-1}x_p)B_l(\eta_p x_p) \end{cases}. \tag{13}$$

The general expression for the characteristic equation of (8) can then be expressed in a compact form as:

$$x_{p+1}\frac{V_{l+1}(\eta_p x_{p+1})}{V_l(\eta_p x_{p+1})} = x_p \frac{x_1 B_{l+1}(x_1)\mathbf{R}_2 - x_2 B_l(x_1)\mathbf{S}_2}{x_1 B_{l+1}(x_1)\mathbf{P}_2 - x_2 B_l(x_1)\mathbf{Q}_2}, \tag{14}$$

where the variables $\mathbf{P}_2$, $\mathbf{Q}_2$, $\mathbf{R}_2$ and $\mathbf{S}_2$ satisfy the recursive relations of (12) and (13). If the number of interfaces is 2, p = 2, then (12) is omitted and the characteristic equation is simply given by (13) and (14). If p = 1, then a classic step-index fiber is obtained and the characteristic equation is directly derived from (10) as

$$x_2\frac{V_{l+1}(x_2)}{V_l(x_2)} = x_1\frac{B_{l+1}(x_1)}{B_l(x_1)}, \tag{15}$$

and, in particular, $n_1 > n_2$ and thus $V = K$, $B = J$, $x_1 = u_1$ and $x_2 = w_2$, leading to the classical step index characteristic equation, [16].

The strategy beyond regrouping terms as in (14) is to intuitively build the characteristic equation of any refractive index profile without the actual need of solving it. Fig. 4 shows a block diagram that summarizes the process to follow in order to reconstruct the characteristic equation of an arbitrary refractive index profile. Starting from the identification of the cladding layer ($k = p$+1), (green box in the upper left corner of Fig. 4), the process proceeds with the analysis of layer 1 (dark yellow elements) and continues with the recursive scheme to analyze each intermediate layer (orange elements) from k = 2 up to p. Following the characteristic equation in (14), this translates into the following process. First, we obtain the left-hand side of (14) for every mode by determining the Bessel function V, the function x_{p+1} and the parameter η_p that define the cladding layer (p+1), (green box). Then, we build the right-hand side of (14) recursively, starting from the first layer (k = 1, dark yellow elements). If the refractive index profile is composed of only 2 layers (i.e., if p = 1), then the characteristic equation is

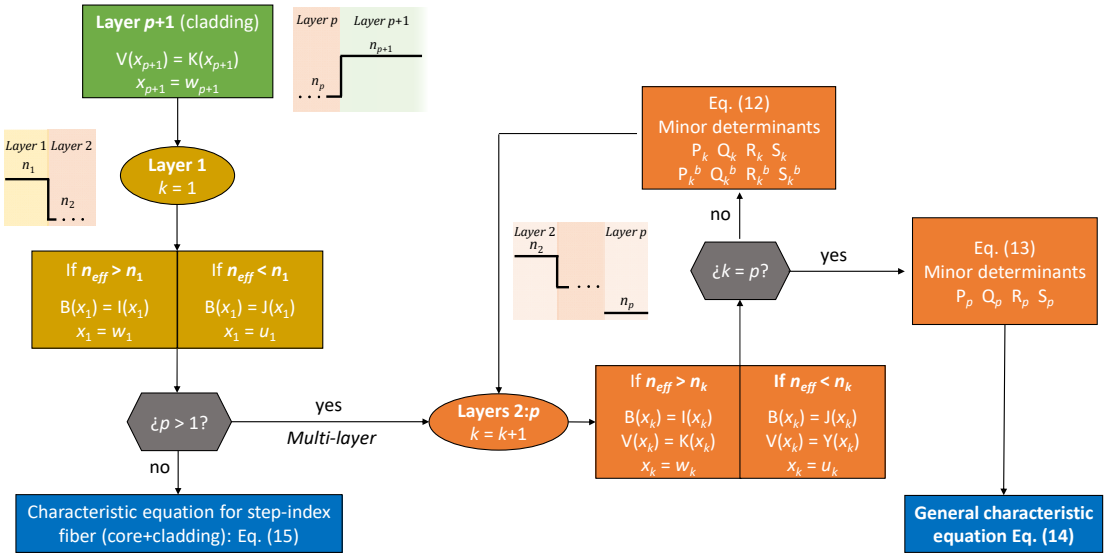

Fig. 4. Block diagram describing the process that reconstructs the characteristic equation of an arbitrary refractive index profile with p+1 concentric layers, as given in (14). Starting from the cladding layer ($k = p$+1), (green box in the upper left corner), the process proceeds with the analysis of layer 1 (dark yellow elements) and continues with the recursive scheme to analyze each intermediate layer (orange elements) from k = 2 up to p.

that of the classic step-index profile given by (15). If $p>1$, then we have to determine, for each intermediate layer k, $2 \le k \le p$ (orange elements), the Bessel functions V and B, the function x_k and the parameter η_k that define that layer, together with the minor determinants $\boldsymbol{P}_k$, $\boldsymbol{Q}_k$, $\boldsymbol{R}_k$, $\boldsymbol{S}_k$, $\boldsymbol{P}_k^b$, $\boldsymbol{Q}_k^b$, $\boldsymbol{R}_k^b$, $\boldsymbol{S}_k^b$. Once the recursive process is finished, i.e., $k = p$, the final characteristic equation is built by combining all these terms as in (14).

III. Derivation of the Main Propagation Parameters

The phase propagation constant of a propagating mode for an arbitrary refractive index profile is obtained from (5) given any of the p+1 eigenvalues u_k/w_k, $k = 1, 2, \ldots, p$+1, of the p+1 layers. In case that (5) is particularized for the highest refractive index layer, $n_{co} = \max_{1\le i\le p}\{n_i\}$, then $n_{eff} < n_{co}$ for every fiber mode (i.e., this layer will always act as core). Let u_{co} be the normalized transverse propagation constant of the highest refractive index profile layer given by (4). Then, the propagation constant is given, for each guided mode, by

$$\beta = k_0 n_{eff} = \sqrt{\left(k_0 n_{co}\right)^2 - \left(u_{co}/a_1\right)^2}. \tag{16}$$

The inverse of the group velocity v_g, which is given by the parameter β_1 ($\beta_1 = v_g^{-1}$), can be derived from (16) as

$$\begin{aligned}\beta_1 &= \frac{d\beta}{d\omega} = \frac{1}{c}\frac{d}{dk_0}\left(\sqrt{k_0^2 n_{co}^2 - \frac{u_{co}^2}{a_1^2}}\right)\\ &= \frac{1}{c\beta}\left[k_0 n_{co}^2 - 2\pi n_{co}\frac{dn_{co}}{d\lambda} + \frac{2\pi}{a_1^2 k_0^2}u_{co}\frac{du_{co}}{d\lambda}\right].\end{aligned} \tag{17}$$

Here, the refractive index n_{co} can be approximated by Sellmeier's equation and, thus, it can be analytically differentiated with respect to the optical wavelength. We see in (17) that the first two terms inside the square brackets do not depend on u_{co}, so they are the same for all modes. The last term depends on both u_{co} and its derivative with respect to the optical wavelength. Since u_{co} must be numerically determined, we must approximate its derivative.

The chromatic dispersion D results from the derivative of β_1 with respect to the optical wavelength. From (17), we get

$$\begin{aligned}D &= \frac{d(\beta_1)}{d\lambda}\\ &= \frac{1}{c\beta}\left[\begin{array}{l} c\frac{\tau_g}{L}\frac{k_0}{\beta}\left(\frac{k}{\lambda}n_{co}^2 - k_0 n_{co}\frac{dn_{co}}{d\lambda} + \frac{1}{a_1^2 k_0}u_{co}\frac{du_{co}}{d\lambda}\right) + \\ \frac{d\left(k_0 n_{co}^2\right)}{d\lambda} - 2\pi\frac{d}{d\lambda}\left(n_{co}\frac{dn_{co}}{d\lambda}\right) + \frac{2\pi}{a_1^2}\frac{d}{d\lambda}\left(\frac{u_{co}}{k_0^2}\frac{du_{co}}{d\lambda}\right)\end{array}\right],\end{aligned} \tag{18}$$

being

$$\frac{d\left(k_0 n_{co}^2\right)}{d\lambda} = -\frac{k_0 n_{co}^2}{\lambda} + 2k_0 n_{co}\frac{dn_{co}}{d\lambda}, \tag{19}$$

$$\frac{d}{d\lambda}\left(n_{co}\frac{dn_{co}}{d\lambda}\right) = \left(\frac{dn_{co}}{d\lambda}\right)^2 + n_{co}\frac{d^2 n_{co}}{d\lambda^2}, \tag{20}$$

$$\frac{d}{d\lambda}\left(\frac{u_{co}}{k_0^2}\frac{du_{co}}{d\lambda}\right) = \frac{\left(\frac{du_{co}}{d\lambda}\right)^2 + u_{co}\left[\frac{d^2 u_{co}}{d\lambda^2} + \frac{2}{\lambda}\frac{du_{co}}{d\lambda}\right]}{k_0^2}. \tag{21}$$

We see again in (18)-(21) that the chromatic dispersion depends on differentiations with respect to the optical wavelength of: (i) n_{co}, which can be solved analytically and are common to all guided modes; and (ii) u_{co}, which have to be numerically approximated and are different for each LP fiber mode.

Equations (16)-(21) are applicable for any multi-layer concentric refractive index profile and, once u_{co} is determined, they are transparent to which profile is being evaluated.

IV. Validation of the Model

Aiming to confirm the validity of the proposed model, we particularize here the general model to four different refractive index profiles and evaluate their propagation characteristics by comparing the results brought by our model with those provided by the commercial numerical solver Fimmwave (from the company Photon Design). Fig. 5 depicts the four optical fiber structures under evaluation: (a) trench-assisted step-index profile, (b) ring-core index profile, (c) four-cladding profile and (d) triangular profile. Green and blue zones delimit, respectively, the areas in which the mode effective index can be lower than the refractive index of a given layer (candidates for core layers), and the area in which the mode effective index is always higher than the refractive index of a given layer (cladding layers).

For each profile, we evaluate the normalized propagation constant b, the group index n_g ($n_g = c\cdot\beta_1$) and the chromatic dispersion D of the non-cutoff modes as a function of the scale factor, which is defined as the parameter that compacts/expands all the refractive index profile radii by the same value given by the scale factor parameter; (a scale factor of 1 leaves invariant the refractive index profile). The normalized propagation constant is defined from (16) as:

$$b = \frac{\left(\beta/k_0\right)^2 - n_{cl}^2}{n_{co}^2 - n_{cl}^2}, \tag{22}$$

where n_{co} is the fiber highest refractive index and n_{cl} is the outer cladding refractive index.

A. Trench-assisted step-index profile

Trench-assisted step-index optical fibers consist of a central core surrounded by an inner cladding region, a trench (or depressed layer) and the outer cladding [3]. We consider the trench-assisted profile of Fig. 5(a), where the material composition of both the inner (n_2) and the outer claddings (n_{cl}) are chosen to be pure silica, the core layer (n_1) is SiO_2 doped with a 5-mol. % of GeO_2 and the lower refractive index of the trench layer (n_3) is achieved by doping the SiO_2 with a 2 mol. % of fluorine (F). The layer radii are $a_1 = 7.5$, $a_2 = 12.5$ and $a_3 = 17.5$ μm. The mode effective indices can vary from n_{cl} up to n_1, and the only layer that can satisfy the condition $n_k > n_{eff}$, ($k = 1, 2, 3$), to act as the fiber core is the first layer, $n_1 = n_{co}$. The normalized transverse propagation constants for each layer are then

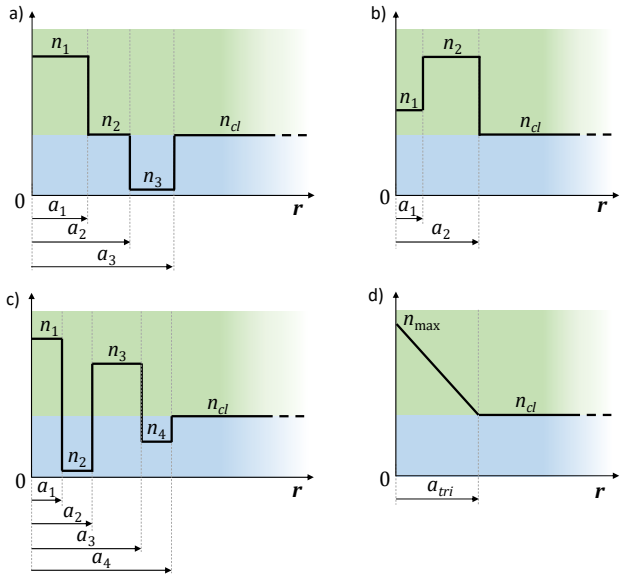

Fig. 5. Particular refractive index profiles evaluated: (a) trench-assisted step-index, (b) ring-core index, (c) four-cladding and (d) triangular-index.

$$u_1 = k_0 a_1 \sqrt{n_1^2 - n_{eff}^2}, \tag{23}$$

$$w_2 = k_0 a_1 \sqrt{n_{eff}^2 - n_2^2}, \tag{24}$$

$$w_3 = k_0 a_1 \sqrt{n_{eff}^2 - n_3^2}, \tag{25}$$

$$w_4 = k_0 a_1 \sqrt{n_{eff}^2 - n_{cl}^2}. \tag{26}$$

The characteristic equation is obtained from the general formula in (14) as:

$$w_4 \frac{K_{l+1}(\eta_3 w_4)}{K_l(\eta_3 w_4)} = w_3 \frac{u_1 J_{l+1}(u_1)\mathbf{R}_2 + w_2 J_l(u_1)\mathbf{S}_2}{u_1 J_{l+1}(u_1)\mathbf{P}_2 + w_2 J_l(u_1)\mathbf{Q}_2}, \tag{27}$$

where the variables $\mathbf{P}_k$, $\mathbf{Q}_k$, $\mathbf{R}_k$ and $\mathbf{S}_k$, $k = 2, 3$, and $\mathbf{P}_2^b$, $\mathbf{Q}_2^b$, $\mathbf{R}_2^b$ and $\mathbf{S}_2^b$ are given by

$$\begin{cases} \mathbf{P}_2 = I_l(w_2)\mathbf{P}_2^b + K_l(w_2)\mathbf{Q}_2^b \\ \mathbf{Q}_2 = I_{l+1}(w_2)\mathbf{P}_2^b - K_{l+1}(w_2)\mathbf{Q}_2^b \\ \mathbf{R}_2 = I_l(w_2)\mathbf{R}_2^b + K_l(w_2)\mathbf{S}_2^b \\ \mathbf{S}_2 = I_{l+1}(w_2)\mathbf{R}_2^b - K_{l+1}(w_2)\mathbf{S}_2^b \end{cases}$$

$$\begin{cases} \mathbf{P}_2^b = w_2 K_{l+1}(\eta_2 w_2)\mathbf{P}_3 + w_3 K_l(\eta_2 x_2)\mathbf{Q}_3 \\ \mathbf{Q}_2^b = w_2 I_{l+1}(\eta_2 w_2)\mathbf{P}_3 - w_3 I_l(\eta_2 x_2)\mathbf{Q}_3 \\ \mathbf{R}_2^b = w_2 K_{l+1}(\eta_2 w_2)\mathbf{R}_3 + w_3 K_l(\eta_2 x_2)\mathbf{S}_3 \\ \mathbf{S}_2^b = w_2 I_{l+1}(\eta_2 w_2)\mathbf{R}_3 - w_3 I_l(\eta_2 x_2)\mathbf{S}_3 \end{cases} \tag{28}$$

$$\begin{cases} \mathbf{P}_3 = I_l(\eta_2 w_3)K_{l+1}(\eta_3 w_3) + K_l(\eta_2 w_3)I_{l+1}(\eta_3 w_3) \\ \mathbf{Q}_3 = I_{l+1}(\eta_2 w_3)K_{l+1}(\eta_3 w_3) - K_{l+1}(\eta_2 w_3)I_{l+1}(\eta_3 w_3) \\ \mathbf{R}_3 = I_l(\eta_2 w_3)K_l(\eta_3 w_3) - K_l(\eta_2 w_3)I_l(\eta_3 w_3) \\ \mathbf{S}_3 = I_{l+1}(\eta_2 w_3)K_l(\eta_3 w_3) + K_{l+1}(\eta_2 w_3)I_l(\eta_3 w_3) \end{cases}.$$

By using (23)-(28), we compute the u_{co} variable and insert it in (16)-(22) to calculate the normalized propagation constant, the group index and the chromatic dispersion of each fiber mode as a function of the scale factor. Fig. 6 compares the results obtained by the present model (solid lines) and those from the commercial solver (dashed lines) for an operation wavelength of $\lambda = 1.55$ μm. The different colors correspond to different LP modes as stated in the legend, where we see the mode profile of each propagating mode. We see an excellent agreement between both solvers in all cases.

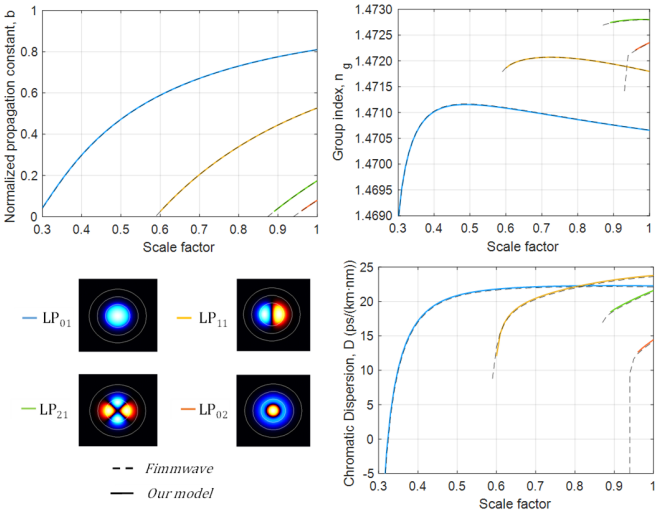

Fig. 6. Normalized propagation constant, group index and chromatic dispersion of each mode as a function of the fiber scale factor for a trench-assisted step-index profile and an operation wavelength of $\lambda = 1.55$ μm. Solid lines correspond to our model and dashed lines to the commercial solver. Bottom-left images: Mode profiles of the propagating modes.

B. Ring-core refractive index profile

Another interesting fiber structure is the ring-core refractive index profile. As opposed to the classic optical fiber structures, here the core (i.e., the layer with the highest refractive index) is not located in the center of the cross-sectional area, [6,7,10,11]. We consider the ring-core optical fiber of Fig. 5(b), with radii $a_1 = 2$ and $a_2 = 9.5$ μm, where the inner hole (n_1) is based on SiO_2 doped with a 2-mol.% of GeO_2 and the core layer (n_2) is doped with a 5-mol.% of GeO_2. The mode effective indices can vary from n_{cl} up to n_2, being $n_{cl} < n_1 < n_2$, and therefore the second layer acts as the fiber core ($n_2 = n_{co}$), while the first layer can act either as core or as cladding. Thus, the normalized transverse propagation constants for each layer are, in this case,

$$\begin{cases} u_1 = k_0 a_1 \sqrt{n_1^2 - n_{eff}^2}, & n_{eff} < n_1 \\ w_1 = k_0 a_1 \sqrt{n_{eff}^2 - n_1^2}, & n_{eff} > n_1 \end{cases} \tag{29}$$

$$u_2 = k_0 a_1 \sqrt{n_2^2 - n_{eff}^2}, \tag{30}$$

$$w_3 = k_0 a_1 \sqrt{n_{eff}^2 - n_{cl}^2}. \tag{31}$$

The characteristic equation is then expressed as:

$$\begin{cases} w_3\dfrac{K_{l+1}(\eta_2 w_3)}{K_l(\eta_2 w_3)}=u_2\dfrac{u_1 J_{l+1}(u_1)\mathbf{R}_2-u_2 J_l(u_1)\mathbf{S}_2}{u_1 J_{l+1}(u_1)\mathbf{P}_2-u_2 J_l(u_1)\mathbf{Q}_2}, & n_{eff}<n_1 \\ w_3\dfrac{K_{l+1}(\eta_2 w_3)}{K_l(\eta_2 w_3)}=u_2\dfrac{w_1 I_{l+1}(w_1)\mathbf{R}_2+u_2 I_l(u_1)\mathbf{S}_2}{w_1 I_{l+1}(w_1)\mathbf{P}_2+u_2 I_l(u_1)\mathbf{Q}_2}, & n_{eff}>n_1 \end{cases} \tag{32}$$

where the variables $\mathbf{P}_2$, $\mathbf{Q}_2$, $\mathbf{R}_2$ and $\mathbf{S}_2$ are given by

$$\begin{cases} \mathbf{P}_2=J_l(u_2)Y_{l+1}(\eta_2 u_2)-Y_l(u_2)J_{l+1}(\eta_2 u_2) \\ \mathbf{Q}_2=J_{l+1}(u_2)Y_{l+1}(\eta_2 u_2)-Y_{l+1}(u_2)J_{l+1}(\eta_2 u_2) \\ \mathbf{R}_2=J_l(u_2)Y_l(\eta_2 u_2)-Y_l(u_2)J_l(\eta_2 u_2) \\ \mathbf{S}_2=J_{l+1}(u_2)Y_l(\eta_2 u_2)-Y_{l+1}(u_2)J_l(\eta_2 u_2) \end{cases}. \tag{33}$$

For an operation wavelength of λ = 1.55 μm, we computed the normalized propagation constant, the group index and the chromatic dispersion of the fiber as a function of the scale factor. Fig. 7 shows the comparison between the results reached via the present model (solid lines) and the ones obtained with the commercial software (dashed lines). The different colors correspond to different LP modes, whose mode profile can be observed in the legend. We see again that both solvers provide mostly identical results for all the parameters evaluated.

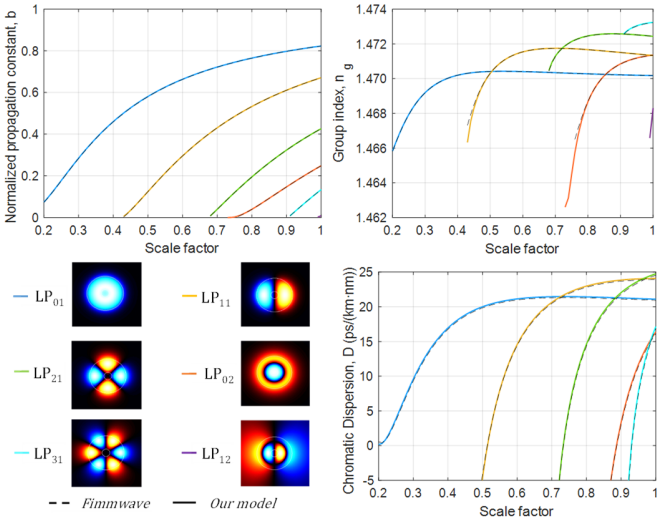

Fig. 7. Normalized propagation constant, group index and chromatic dispersion of each mode as a function of the fiber scale factor for a ring-core index profile and an operation wavelength of λ = 1.55 μm. Solid lines correspond to our model and dashed lines to the commercial solver. Bottom-left images: Mode profiles of the propagating modes.

C. *Four-cladding refractive index profile*

More complex refractive index profiles comprise a higher number of layers, as the four-cladding refractive index profile shown in Fig. 5(c). Here, the core layer is centered in the fiber cross-section, and it is surrounded by a combination of a depressed trench, an upper-index ring and a second trench layer, [14,15]. We consider again pure silica for the infinite outer cladding region. Both the core layer (n_1) and the ring (n_3) are doped with GeO_2 (5 mol.% for the core and 3 mol.% for the ring), while the depressed index for the trenches are achieved by doping the SiO_2 with Fluorine (2-mol.% for the inner trench, n_2, and 1-mol.% for the outer trench, n_4). We set the radii to 4, 8, 16 and 20 μm, respectively for a_1, a_2, a_3 and a_4. The normalized transverse propagation constants are then

$$u_1=k_0 a_1\sqrt{n_1^2-n_{eff}^2}, \tag{34}$$

$$w_2=k_0 a_1\sqrt{n_{eff}^2-n_2^2}, \tag{35}$$

$$\begin{cases} u_3=k_0 a_1\sqrt{n_3^2-n_{eff}^2}, & n_{eff}<n_3, \\ w_3=k_0 a_1\sqrt{n_{eff}^2-n_3^2}, & n_{eff}>n_3, \end{cases} \tag{36}$$

$$w_4=k_0 a_1\sqrt{n_{eff}^2-n_4^2}. \tag{37}$$

$$w_5=k_0 a_1\sqrt{n_{eff}^2-n_{cl}^2}. \tag{38}$$

The characteristic equation is obtained from Eq. (14) as:

$$w_5\frac{K_{l+1}(\eta_4 w_5)}{K_l(\eta_4 w_5)}=w_4\frac{u_1 J_{l+1}(u_1)\mathbf{R}_2-w_2 J_l(u_1)\mathbf{S}_2}{u_1 J_{l+1}(u_1)\mathbf{P}_2-w_2 J_l(u_1)\mathbf{Q}_2}, \tag{39}$$

where the variables $\mathbf{P}_k$, $\mathbf{Q}_k$, $\mathbf{R}_k$ and $\mathbf{S}_k$, k = 2, 3, 4, and $\mathbf{P}_k{}^b$, $\mathbf{Q}_k{}^b$, $\mathbf{R}_k{}^b$ and $\mathbf{S}_k{}^b$, k = 2, 3, are given by

$$\begin{cases} \mathbf{P}_2=-I_l(w_2)\mathbf{P}_2^b-K_l(w_2)\mathbf{Q}_2^b \\ \mathbf{Q}_2=I_{l+1}(w_2)\mathbf{P}_2^b-K_{l+1}(w_2)\mathbf{Q}_2^b \\ \mathbf{R}_2=-I_l(w_2)\mathbf{R}_2^b-K_l(w_2)\mathbf{S}_2^b \\ \mathbf{S}_2=I_{l+1}(w_2)\mathbf{R}_2^b-K_{l+1}(w_2)\mathbf{S}_2^b \end{cases}, \tag{40}$$

$n_{eff}>n_3$	$n_{eff}<n_3$
$\begin{cases} \mathbf{P}_2^b=w_2K_{l+1}(\eta_2 w_2)\mathbf{P}_3-w_3K_l(\eta_2 w_2)\mathbf{Q}_3 \\ \mathbf{Q}_2^b=w_2I_{l+1}(\eta_2 w_2)\mathbf{P}_3+w_3I_l(\eta_2 w_2)\mathbf{Q}_3 \\ \mathbf{R}_2^b=w_2K_{l+1}(\eta_2 w_2)\mathbf{R}_3-w_3K_l(\eta_2 w_2)\mathbf{S}_3 \\ \mathbf{S}_2^b=w_2I_{l+1}(\eta_2 w_2)\mathbf{R}_3+w_3I_l(\eta_2 w_2)\mathbf{S}_3 \end{cases}$	$\begin{cases} \mathbf{P}_2^b=w_2K_{l+1}(\eta_2 w_2)\mathbf{P}_3-u_3K_l(\eta_2 w_2)\mathbf{Q}_3 \\ \mathbf{Q}_2^b=w_2I_{l+1}(\eta_2 w_2)\mathbf{P}_3+u_3I_l(\eta_2 w_2)\mathbf{Q}_3 \\ \mathbf{R}_2^b=w_2K_{l+1}(\eta_2 w_2)\mathbf{R}_3-u_3K_l(\eta_2 w_2)\mathbf{S}_3 \\ \mathbf{S}_2^b=w_2I_{l+1}(\eta_2 w_2)\mathbf{R}_3+u_3I_l(\eta_2 w_2)\mathbf{S}_3 \end{cases}$
$\begin{cases} \mathbf{P}_3=-I_l(\eta_2 w_3)\mathbf{P}_3^b-K_l(\eta_2 w_3)\mathbf{Q}_3^b \\ \mathbf{Q}_3=I_{l+1}(\eta_2 w_3)\mathbf{P}_3^b-K_{l+1}(\eta_2 w_3)\mathbf{Q}_3^b \\ \mathbf{R}_3=-I_l(\eta_2 w_3)\mathbf{R}_3^b-K_l(\eta_2 w_3)\mathbf{S}_3^b \\ \mathbf{S}_3=I_{l+1}(\eta_2 w_3)\mathbf{R}_3^b-K_{l+1}(\eta_2 w_3)\mathbf{S}_3^b \end{cases}$	$\begin{cases} \mathbf{P}_3=J_l(\eta_2 u_3)\mathbf{P}_3^b-Y_l(\eta_2 u_3)\mathbf{Q}_3^b \\ \mathbf{Q}_3=J_{l+1}(\eta_2 u_3)\mathbf{P}_3^b-Y_{l+1}(\eta_2 u_3)\mathbf{Q}_3^b \\ \mathbf{R}_3=J_l(\eta_2 u_3)\mathbf{R}_3^b-Y_l(\eta_2 u_3)\mathbf{S}_3^b \\ \mathbf{S}_3=J_{l+1}(\eta_2 u_3)\mathbf{R}_3^b-Y_{l+1}(\eta_2 u_3)\mathbf{S}_3^b \end{cases}$
$\begin{cases} \mathbf{P}_3^b=w_3K_{l+1}(\eta_3 w_3)\mathbf{P}_4-w_4K_l(\eta_3 w_3)\mathbf{Q}_4 \\ \mathbf{Q}_3^b=w_3I_{l+1}(\eta_3 w_3)\mathbf{P}_4+w_4I_l(\eta_3 w_3)\mathbf{Q}_4 \\ \mathbf{R}_3^b=w_3K_{l+1}(\eta_3 w_3)\mathbf{R}_3-w_4K_l(\eta_3 w_3)\mathbf{S}_3 \\ \mathbf{S}_3^b=w_3I_{l+1}(\eta_3 w_3)\mathbf{R}_3+w_4I_l(\eta_3 w_3)\mathbf{S}_3 \end{cases}$	$\begin{cases} \mathbf{P}_3^b=u_3Y_{l+1}(\eta_3 u_3)\mathbf{P}_4-w_4Y_l(\eta_3 u_3)\mathbf{Q}_4 \\ \mathbf{Q}_3^b=u_3J_{l+1}(\eta_3 u_3)\mathbf{P}_4-w_4J_l(\eta_3 u_3)\mathbf{Q}_4 \\ \mathbf{R}_3^b=u_3Y_{l+1}(\eta_3 u_3)\mathbf{R}_4-w_4Y_l(\eta_3 u_3)\mathbf{S}_4 \\ \mathbf{S}_3^b=u_3J_{l+1}(\eta_3 u_3)\mathbf{R}_4-w_4J_l(\eta_3 u_3)\mathbf{S}_4 \end{cases}$

(41)

$$\begin{cases} \mathbf{P}_4=-I_l(\eta_3 w_4)K_{l+1}(\eta_4 w_4)-K_l(\eta_3 w_4)I_{l+1}(\eta_4 w_4) \\ \mathbf{Q}_4=I_{l+1}(\eta_3 w_4)K_{l+1}(\eta_4 w_4)-K_{l+1}(\eta_3 w_4)I_{l+1}(\eta_4 w_4) \\ \mathbf{R}_4=-I_l(\eta_3 w_4)K_l(\eta_4 w_4)+K_l(\eta_3 w_4)I_l(\eta_4 w_4) \\ \mathbf{S}_4=I_{l+1}(\eta_3 w_4)K_l(\eta_4 w_4)+K_{l+1}(\eta_3 w_4)I_l(\eta_4 w_4) \end{cases}. \tag{42}$$

Fig. 8 compares the normalized propagation constant, the group index and the chromatic dispersion computed from both the present solver (solid lines) and the commercial solver (dashed lines) for an operation wavelength of λ = 1.55 μm. The different colors correspond to different LP modes, whose mode

profiles are shown in the legend. Once again, both solvers present almost identical results in all cases.

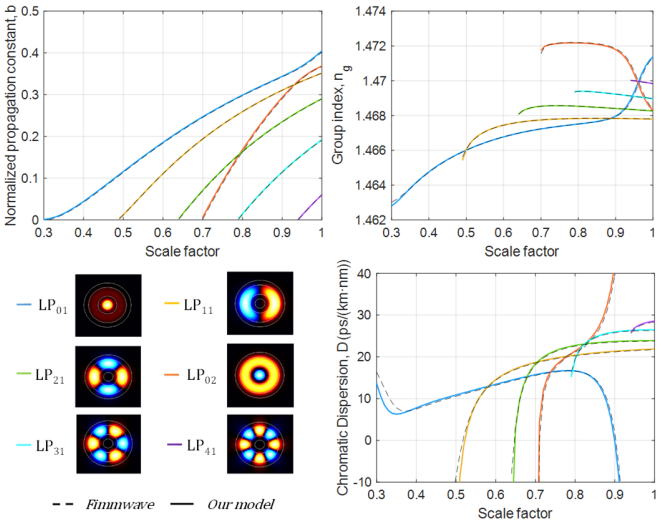

Fig. 8. Normalized propagation constant, group index and chromatic dispersion of each mode as a function of the fiber scale factor for a four-cladding refractive index profile and an operation wavelength of λ = 1.55 µm. Solid lines correspond to our model and dashed lines to the commercial solver. Bottom-left images: Mode profiles of the propagating modes.

D. Triangular refractive index profile

Finally, we study the viability of analyzing continuous (or non-stepped) refractive index profiles with the present model. First, we prove that a proper step-index discretization converges rapidly to the continuous profile. In particular, we consider the triangular refractive index profile, [13] depicted in of Fig. 5(d), where the refractive index at $r = 0$ has a material composition of SiO_2 doped with a 5-mol.% GeO_2 and decreases linearly with the radii until reaching the pure silica of the cladding region at the radius $a_{tri} = 10$ µm.

We study how to discretize the triangular profile by an n-step index profile with equal-width steps and in which the material composition of each step decreases linearly with the step number. We can consider the superior discretization, in which each layer k, (k = 1, 2, …, n), is created by extending the corresponding value of the triangular function at $r = (k\text{-}1)\cdot 10/n$ up to the radius $r = k\cdot 10/n$. In a similar way, we can also consider the inferior discretization in which each layer k, (k = 1, 2, …, n), is created by extending the corresponding value of the triangular function at $r = k\cdot 10/n$ down to the radius $r = (k\text{-}1)\cdot 10/n$. It is clear that both the superior and the inferior discretization tend to the triangular profile when n tends to infinity, and they correspond exactly to the superior and inferior limits of this linear step-index discretization, respectively. It is then reasonable to consider the half-point discretization, in which we extend the value of the index at $r = (k\text{-}1/2)\cdot 10/n$ from $r = (k\text{-}1)\cdot 10/n$ up to the radius $r = k\cdot 10/n$. Obviously, since this function is in-between the superior and inferior functions, it also converges to the triangular profile, and it is logical to think that it will converge faster than both the superior and the inferior discretization. Fig. 9(a) depicts the comparison between all three functions for n = 5 steps. Red-dashed line corresponds to the superior (f_{sup}), blue-dashed to the inferior (f_{inf}), and green-solid to the medium function (f_{tri}). We can also observe that as long as n increases, the medium function converges rapidly to the triangular profile, as the purple dotted-line curve shows for n = 10 steps. Fig. 9(b) shows the convergence on the propagation constant computed for the discretized profile (f_{tri}) as a function of the number of discretization steps n for the propagating modes. As we observe in the zoomed area in the inset of Fig. 9(b), the propagation constant mismatch for n = 10 steps is below 10^{-5} for both propagating modes, which is almost negligible, while the convergence for n = 5 is still acceptable, with a difference below $5\cdot 10^{-5}$. This shows that the discretized profile converges adequately to the ideal response even with a very low number of steps.

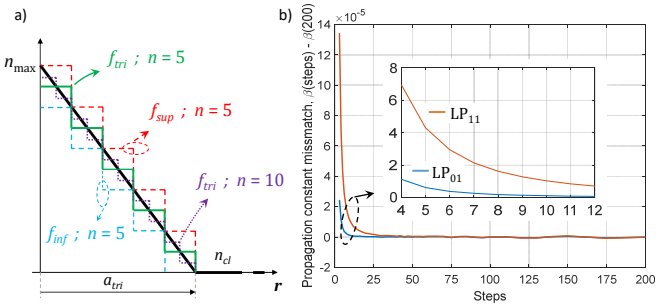

Fig. 9. (a) Discretization of the triangular refractive index profile; (b) Convergence of the propagation constant on the discretized triangular refractive index profile as a function of the discretization steps.

Once we prove the convergence of the discretized triangular profile, we evaluate the particular case in which the number of discretization steps is set to 5. In this case, for simplicity, we avoid the expression of the characteristic equation. However, the construction in this case is very simple: since the refractive index profile is a monotonically decreasing function with the radius, all layers with layer number below a given layer k, (k = 1, 2, … 5), will satisfy the condition $n_k > n_{eff}$, and thus will act as core layers; layers numbered higher than k will then act as cladding layers. The characteristic equation is then formed in a similar way than the rest of the examples evaluated before. Fig. 10 compares the computed normalized propagation constant, the group index and the chromatic dispersion as a function of the scale factor for both the proposed method and the commercial solver at λ = 1.55 µm. The mode profiles for both propagating modes are given in the legend. As in the previous examples, we see again an excellent agreement between both solvers for all of the parameters.

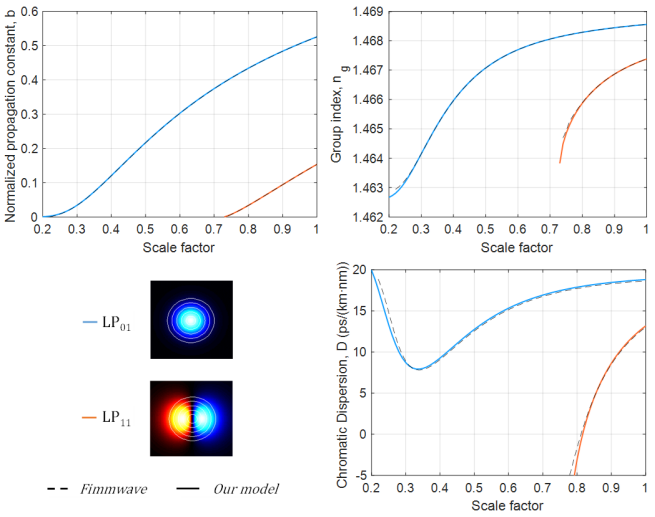

Fig. 10. Normalized propagation constant, group index and chromatic dispersion of each mode as a function of the fiber scale factor for a triangular index profile and an operation wavelength of λ = 1.55 μm. Solid lines correspond to our model and dashed lines to the commercial solver. Bottom-left images: Mode profiles of the propagating modes.

V. Discussion on the Model Applicability Domain

The model we report in this work applies in general to multi-layer optical fibers comprising any number of concentric circular layers, where each layer has arbitrary radial dimensions as well as an arbitrary refractive index n_k with a constant value among that layer. This applies directly to discrete or stepped refractive index profiles, as step-index profiles comprising different trench and/or core structures. As we have seen in section IV, continuous refractive index profiles can also be evaluated through this model if a discretization of the continuous segment of the profile is properly done. Although we demonstrated a fast convergence of the results for a triangular profile, this method can also be applied for instance to graded-index profiles, [12,20], with a similar convergence rate.

For any of the structures mentioned above, we can also use this model to calculate their cladding modes by simply adding an additional infinite external cladding and limiting the previous outer cladding to a finite value. The simplest example is the case of a classic step-index optical fiber with a single layer (p = 1) and the outer cladding region. We can compute the cladding modes if we restrict the outer cladding to a finite value (for example, a_2 = 62.5 μm) and include a new infinite external cladding (such as an air layer, for instance). Then, we can solve the characteristic equation of this new 2-layer structure (p = 2) via (14) and obtain the propagating modes. The cladding modes of the initial monolayer structure correspond to the new modes that propagate in the bilayer structure that were in cutoff in the first one.

We must take into account that this model applies to symmetrical optical fibers in the azimuthal direction (i.e., concentric layers), as the ones discussed in this work. In case, for instance, of core structures that are surrounded by air holes, (such as hole-assisted [21] or hole-walled [22] fibers), or elliptical fibers, one has to resort to numerical software tools. Although we have evaluated only single-core fibers, the propagation characteristics of multicore fibers can also be assessed if the refractive index profile of the different cores are treated as independent entities, [23]. This is the situation of weakly coupled multicore fibers where the level of intercore crosstalk is low enough as to the model each core individually (under the assumption, as always, of infinite outer cladding region and the use of local coordinates for each core). In that regard, our model is effective for the design of each one of the cores (specially in heterogeneous multicore schemes), while the crosstalk performance can be computed from the coupled power theory [24], where in turn the average power coupling coefficient depends on the propagation parameters provided by our model.

VI. Conclusions

We have presented, for the first time to our knowledge, a theoretical model deriving the universal characteristic equation for multi-layer optical fibers whose refractive index profile comprises any number of concentric circular layers with arbitrary radial dimensions and refractive index values. The closed-form expression we derived for the characteristic equation provides a useful tool to obtain relevant information about the propagation characteristics of all the propagated much, such as the phase propagation constant, group delay and the chromatic dispersion. The model can be applied to both flat (or stepped) refractive index profiles (such as step-index, W-type or ring-core) and continuous profiles (such as graded-index or triangular) if a previous discretization process is applied properly. The validity of the proposed model has been accomplished by comparing the results offered by our theory with the ones provided by the numerical software Fimmwave form Photon Design for four different profiles: step-index trench-assisted, ring-core, triangular-index and four-cladding. Excellent agreement is obtained in all the cases in terms of the normalized propagation constant, group index and chromatic dispersion for all the modes propagated.

The compact characteristic equation we present here will play an important role in optical fiber design processes, where the designer can actually get valuable physical insights without the need of resorting to numerical software tools. While other methods are based on the “brute force” resolution of Maxwell’s equations without having any knowledge about the functions involved, our model enables to build the overall characteristic equation that defines wave propagation. More importantly, one can benefit from the possibility of evaluating the effect of the properties of a particular layer on the performance of the propagated modes without the need to evaluate the whole refractive index structure, since one has knowledge about the functions that are involved in that layer, as we can see in (12)-(14).

All in all, the advantages brought by this universal characteristic equation will benefit a variety of optical communications and signal processing scenarios where multi-layer fibers are particularly needed, such as space and mode-division multiplexing, fiber sensing, optical interconnects, loss and dispersion management, as well as high-power amplifiers and lasers.

REFERENCES

[1] K. C. Kao and G. A. Hockham, "Dielectric-Fibre Surface Waveguides for Optical frequencies," in *Proc. IEE*, vol. 113, no. 7, pp. 1151-1158, 1966.

[2] G. P. Agrawal, *Fiber-Optic Communications systems*, 4th ed., John Wiley & Sons, 2010.

[3] M. Monerie, "Propagation in doubly clad single-mode fibers," *J. of Quantum Electron.*, vol. 18, no. 4, pp. 535-542, 1982.

[4] K. Mikoshiba and H. Kajioka, "Transmission characteristics of multimode W-type optical fiber: experimental study of the effect of the intermediate layer," *Appl. Opt.*, vol. 17, pp. 2836-2841, 1978.

[5] S. Kawakami and S. Nishida, "Characteristics of a doubly clad optical fiber with a low-index inner cladding," *J. of Quantum Electron*., vol. 10, no. 12, pp. 879-887, 1974.

[6] S. Kawakami, S. Nishida and M. Sumi, "Special issue paper. Transmission characteristics of W-type optical fibres," in *Proc. IEE*, vol. 123, no. 6, pp. 586-590, 1976.

[7] E. Snitzer, H. Po, F. Hakimi, R. Tumminelli, and B. C. McCollum, "Double clad, offset core Nd fiber laser," in *Proc. of Optical Fiber Sensors*, vol. 2, (Optical Society of America, 1988), paper PD5.

[8] X. Jin et al., "Mode coupling effects in ring-core fibres for space-division multiplexing systems," *J. of Lightw. Technol*., vol. 34, no. 14, pp. 3365-3372, 2016.

[9] R. Romaniuk, "Basic properties of ring-index optical fibers," in *Proc. SPIE 5028 Optical Fibers and Their Applications VIII*, 2003, pp. 19-25.

[10] V. Pelodya and S. K. Raghuwanshi, "Design and parametric study of depressed core optical fiber," in *Int. Conf. on Inform. and Comm. Technol. (ICICT 2014)*, Kochi, India, 2014, pp. 1385-1392.

[11] M. Hautakorpi and M. Kaivola, "Modal analysis of M-type-dielectric-profile optical fibers in the weakly guiding approximation," *J. Opt. Soc. Am. A*, vol. 22, no. 6, pp. 1163-1169, 2005.

[12] P. Sillard, M. Bigot-Astruc and D. Molin, "Few-Mode Fibers for Mode-Division-Multiplexed Systems," *J. Lightw. Technol.,* vol. 32, no. 16, pp. 2824-2829, 2014.

[13] B. Ainslie and C. Day, "A review of single-mode fibers with modified dispersion characteristics," *J. Lightw. Technol.*, vol. 4, no. 8, pp. 967-979, 1986.

[14] P. L. Francois, "Propagation mechanisms in quadruple-clad fibres: mode coupling, dispersion and pure bend losses," *Electron. Lett*., vol. 19, no. 21, pp. 885-886, 1983.

[15] L. de Montmorillon, P. Sillard, M. Astruc-Bigot, B. Dany, P. Nouchi, B. Lavigne, E. Balmefrezol, J. Antona, and O. Leclerc, "Transmission Fiber Optimized for Metro Optical Network," in *Optical Fiber Communication Conference and Exposition and The National Fiber Optic Engineers Conference*, Technical Digest (CD) (Optical Society of America, 2005), paper OFH1.

[16] D. Gloge, "Weakly Guiding Fibers," *Appl. Opt.*, vol. 10, no. 10, pp. 2252-2258, 1971.

[17] P. R. Watekar, S. Ju, L. Htein, and W. T. Han, "A simple and reliable method to determine LP_{11} cutoff wavelength of bend insensitive fiber," *Opt. Exp.*, vol. 18, no. 13, pp. 13761-13771, 2010.

[18] S. Kawakami and S. Nishida, "Perturbation theory of a doubly clad optical fiber with a low-index inner cladding," *J. of Quantum Electron*., vol. Q-e-11, no. 4, pp. 130-138, 1975.

[19] K. Okamoto, "Fundamentals of optical waveguides," *Academic Press*, 2006.

[20] D. Gloge and E. A. J. Marcatili, "Multimode theory of graded-core fibers," *The Bell System Technical J*., vol. 52, no. 9, pp. 1563-1578, 1973.

[21] K. Saitoh, T. Matsui, T. Sakamoto, M. Koshiba and S. Tomita, "Multi-core hole-assisted fibers for high core density space division multiplexing," in *OECC 2010 Technical Digest*, Sapporo, 2010, 164-165.

[22] B. Yao, "Reduction of Crosstalk by Hole-Walled Multi-Core Fibers," in *Optical Fiber Communication Conference*, OSA Technical Digest (Optical Society of America, 2012), paper OM2D.5.

[23] D. J. Richardson, J. M. Fini, and L. E. Nelson, "Space-division multiplexing in optical fibres," *Nat. Photonics,* vol. 7, pp. 354-362, 2013.

[24] M. Koshiba, K. Saitoh, K. Takenaga, and S. Matsuo, "Analytical expression of average power-coupling coefficients for estimating intercore crosstalk in multicore fibers," *IEEE Photonics J.*, vol. 4, no. 5, pp. 1987-1995, 2012.

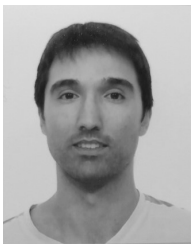

Sergi García received the B.Sc. degree in telecommunications and the M.Sc. degree in telecommunication technologies, sys tems and networks in 2014 and 2015, respectively, both from Universitat Politècnica de València (UPV), Valencia, Spain. He is currently studying the B.Sc. degree in mathematics from Universidad Nacional de Educación a Distancia, Spain, and working towards the Ph.D. degree in telecommunications with the Photonics Research Labs group at the iTEAM research institute, UPV. His current research interests are focused on the application of space division multiplexing technologies in both multicore and few-mode fibers to Microwave Photonics.

Ivana Gasulla (M'07–SM'16) received the M. Sc. degree in Telecommunications Engineering and the Ph.D. degree in Telecommunications from the Universitat Politècnica de València (UPV), Spain, respectively, in 2005 and 2008. She is currently a senior researcher (Ramon y Cajal Fellow) and deputy director for Dissemination and Promotion at the iTEAM Research Institute of UPV. In 2016, she was awarded a prestigious ERC Consolidator Grant to develop new Space-Division Multiplexing technologies for emergent fiber-wireless communications through the project InnoSpace. Her current research interests encompass, among others, the application of multimode and multicore fibers to Microwave Photonics systems. The results of her work have led to more than 100 international publications, highlighting contributions to Nature Communications and Nature Photonics. She is a member of the TPC of the most prestigious conferences in the field: European Conference on Optical Communications (ECOC), Optical Fiber Communication Conference (OFC) and IEEE International Topical meeting on Microwave Photonics (MWP), among others.